Fuel 366 (2024) 131381

Contents lists available at ScienceDirect

Fuel

journal homepage: www.elsevier.com/locate/fuel

Full length article

Radiating biofuel-blended turbulent nonpremixed hydrogen flames on a coaxial spray burner

Yilong Yin [a,*], Paul R. Medwell [a], Bassam B. Dally [b]

[a] School of Electrical and Mechanical Engineering, The University of Adelaide, Adelaide, South Australia 5005, Australia
[b] Clean Combustion Research Centre, King Abdullah University of Science and Technology, Thuwal 23955-6900, Kingdom of Saudi Arabia

ARTICLE INFO

Keywords:
Hydrogen flame
Biofuel surrogate
Needle spray burner
Radiative heat flux
Gas-assist atomisation

ABSTRACT

The low radiant intensity and luminosity of hydrogen flames can be enhanced by the addition of a small portion of sooting biofuels. To achieve higher effectiveness, the impact of blending turbulent nonpremixed hydrogen flames with liquid biofuels, by gas-assist atomisation, is investigated and compared with the introduction methods of prevapourisation and ultrasonic spray. The flame appearance, luminosity, radiant fraction, centreline temperature, and the near-field spray characteristics of four biofuel surrogates (eucalyptol, D-limonene, guaiacol, and anisole) blended into hydrogen flames are measured experimentally. Radiating biofuel/hydrogen flames are achieved on a coaxial needle spray burner by the addition of 0.1–0.3 mol% biofuel surrogates. Compared with the unblended hydrogen flame, the luminosity and radiant fraction are enhanced by 30%–500% and 2%–15%, respectively, with the addition of biofuel surrogates. The results show that adding the biofuel surrogates by gas-assist atomisation is more effective than prevapourisation and ultrasonic atomisation in luminosity and radiant fraction enhancement. It is found that the local fuel-rich conditions, which are beneficial for soot formation, are further facilitated by the larger droplets and spray objects generated by gas-assist atomisation. Of the additives tested, anisole is the most effective for luminosity and radiant fraction enhancement of a hydrogen flame while exhibiting the largest flame temperature drop due to the enthalpy of vapourisation and the radiative loss from the promoted soot formation. The viscosity and surface tension greatly influence the spray characteristics which in turn impacts the flame characteristics. Guaiacol, the representative of lignin, appears to have the lowest effectiveness in radiant fraction enhancement due to the presence of a hydroxy group, a higher bond dissociation enthalpy, and a coarser spray ascribed to higher viscosity and surface tension.

1. Introduction

In recent years, hydrogen has been increasingly recognised as a promising energy carrier capable of replacing fossil fuels in industrial processes, driven by the urgent need to mitigate greenhouse gas emissions. This burgeoning interest in hydrogen arises from its potential to offer a clean and sustainable energy alternative, owing to its ability to produce only water vapour when consumed. However, this carbon-free nature of hydrogen flames gives rise to a noteworthy challenge for practical applications—their diminished radiant intensity renders hydrogen flames inadequate for many industrial combustion systems, which typically depend on radiative heat transfer as a primary means of heat transfer. In stationary energy systems, such as furnaces and boilers, thermal radiation commonly serves as the predominant mode of heat transfer, notably enhanced by the effective blackbody radiation emitted from soot particles. Although gaseous constituents (e.g. CO_2 and H_2O) also play a role in thermal radiation, their contribution is generally minor compared with the radiative heat transfer from soot particulates [1–3]. These combustion systems typically feature a radiant section as a primary configuration designed to capture thermal heat emitted from the flames [4,5]. To address the diminished radiant intensity exhibited by hydrogen flames, a viable strategy involves incorporating a small fraction of sooting biofuels into the hydrogen blend [4,6]. This intentional blending serves to augment the radiative heat flux by facilitating the formation of soot particles [1,7–10].

The effectiveness of promoting soot formation and the consequent radiant intensity is subject to the influence of numerous factors. These factors encompass a wide range of parameters that can impact the process, including but not limited to residence time, flame temperature, and the properties of additives [11–20]. It has been reported that blending turbulent hydrogen flames with various biofuels at less than 1 mol% (based on the mole concentration of H_2) by prevapourisation and

* Corresponding author.
E-mail address: yilong.yin@adelaide.edu.au (Y. Yin).

https://doi.org/10.1016/j.fuel.2024.131381
Received 3 November 2023; Received in revised form 26 February 2024; Accepted 28 February 2024
Available online 5 March 2024
0016-2361/© 2024 The Authors. Published by Elsevier Ltd. This is an open access article under the CC BY license (http://creativecommons.org/licenses/by/4.0/).

ultrasonic atomisation does not achieve sooting flames and the largest radiant fraction enhancement was found at 19% in toluene/hydrogen blends [9,10]. Further increasing the concentration of toluene in the hydrogen blends to 4 mol% greatly promotes soot formation and alters the flame appearance from blue to yellow colouration [10]. The radiant fraction increases by 33% compared with the non-blended hydrogen flame. Amongst the various biofuels studied, non-oxygenated biofuels with aromatic structures tend to favour soot formation compared with oxygenated fuels and monoterpenes [1,8–10,21].

Apart from influencing factors of additives' chemical properties and concentrations, the method of introducing additives to the hydrogen flame affects the phase and morphology of the additive, therefore impacting soot formation and radiant intensity enhancement due to altered mixing mechanisms. Spray additives produce more soot compared with prevapourised additives because fuel-rich regions created by a spray favour soot formation [1]. However, changing the introduction method from prevapourisation to ultrasonic spray has a moderate effect on the radiant intensity enhancement of biofuel-blended hydrogen flames [10]. The liquid droplets generated by ultrasonic atomisation are fine, at about 30 μm diameter [1,10,22]. It is hypothesised that larger liquid fuel droplets may be needed to further enhance the local fuel-rich conditions for promoting soot formation. In addition, the use of ultrasonic nebuliser for atomisation induces complexity to application and limits the liquid fuel additives since it is sensitive to purity and physical properties of the fuel. Therefore, investigating an introduction method of the additive with the potential for further enhancing soot formation while maintaining the spray flame stability becomes the motivation of this investigation.

Amongst various methods of liquid fuel atomisation, gas-assist atomisation driven by the airblast effect has the most potential as the liquid droplet size can be controlled by atomisation conditions, hence capable of forming larger droplets. In addition, the simplicity of the gas-assist atomisation configuration and the insensitivity to liquid with various physical properties benefit its application in liquid fuel combustion. Gas-assist atomisation can be described as the process of dispersing individual liquid droplets within a gaseous medium, wherein these droplets undergo progressive evolution facilitated by the interactions of turbulent dispersed two-phase flow phenomena [23,24]. When a liquid flow is introduced into a gaseous medium, the interface between the two flows, characterised by varying velocities or densities, gives rise to Kelvin–Helmholtz instabilities. These instabilities promote the amplification of Rayleigh–Taylor instabilities. Immediately upon exiting the nozzle, deformations emerge on the liquid interface, which subsequently evolve in size and magnitude over both distance and time. The presence of deformations and disturbances on the liquid flow surface initiates oscillations characterised by dilation and wave structures. These oscillations lead to the fragmentation of the liquid flow into ligaments, large droplets, and irregular objects, constituting the primary breakup mechanism. This primary breakup predominantly occurs in the vicinity of the nozzle exit, representing a region of dense spray regime, wherein the dynamics are primarily governed by fragment coalescence and collision. Subsequently, as the liquid fragments progress downstream, they encounter aerodynamic forces that trigger a secondary breakup mechanism. In this mechanism, the fragments experience further disintegration into smaller elements, with minimal droplet-to-droplet interactions occurring [25,26].

Dual concentric jets burners are commonly employed to perform gas-assist atomisation and establishing gas/liquid blended flames. The spray characterisation involves using techniques such as laser Doppler velocimetry (LDV), phase Doppler particle anemometry (PDPA), and microscopic shadowgraph imaging to investigate the break-up morphology of liquid streams under various gas/liquid conditions, including breakup length, ligaments, and droplets. In comparison to spray characterisation, multi-phase reacting flows are relatively poorly understood due to the challenge of stabilising the flame. There is a risk of unconsumed atomised liquid fuel droplets escaping from the flame when excessively large droplets are formed in coarse sprays as a result of the inappropriate design of atomisation conditions (e.g. non-dimensional parameters such as gas/liquid momentum flux ratio). The physical properties of the liquid fuel play an important role in gas-assist atomisation, including viscosity, surface tension, and density, which in turn affect flame stability. In addition, the combustion properties of the liquid fuel are also the critical factors contributing to flame stability, namely flammability and volatility. The blow-off limit and the corresponding flame stability have been investigated on dual concentric jet burners using highly flammable gaseous fuels and liquid fuels (e.g. acetone and ethanol) with a piloted flame [26]. There is a lack of research that has reported on utilising the gas-assist atomisation of liquid biofuels for enhancing the radiant intensity of hydrogen flames. As mentioned, soot formation favours larger liquid droplets for creating fuel-rich conditions, which raises challenges of balancing the form of larger liquid droplets in a coarse spray for the effectiveness of radiant intensity enhancement, and the impact of larger liquid droplets on flame stability.

Liquid biofuels are suitable soot-enhancing additives as they are biomass-derived renewable fuels with high sooting propensities. Bio-oil and essential oil are two major categories of biofuels which commonly comprise aromatics and terpene, respectively. Since bio-oil and essential oil contain complex compounds, surrogates are needed to emulate the chemical, physical, and combustion properties of the biofuels for chemical analysis [27–29]. Four biofuel surrogates are selected in this paper, with their chemical structures shown in Fig. 1. Anisole (C_7H_8O) and guaiacol ($C_7H_8O_2$) are chosen as the surrogates for bio-oil since their chemical structures and functional groups are representative of the lignin patterns [30]. They both are oxygenated fuels containing a methoxy group (-OCH_3) which is a typical functional group of bio-oil derived by fast pyrolysis. The additional hydroxyl group in guaiacol compared with anisole allows the investigation of its effect on soot formation. Eucalyptol ($C_{10}H_{18}O$) and D-limonene ($C_{10}H_{16}$) are selected as the surrogates for essential oils as they are the primary component of eucalyptus oil and orange oil, respectively [31,32]. The effectiveness of blending these monoterpenes on soot formation can be compared with aromatics to deepen the understanding of the potential application of biofuels.

The fundamental understanding of the sooting propensities of the potential biofuel additives and their effect of phase and concentration on the biofuel-blended hydrogen flames have been established. However, the influence on flame characteristics and radiant intensity enhancement is limited. The gaps in understanding various biofuel surrogates, and how the introduction method and mixing mechanism will have impacts on the blending effect still remain. In this paper, the efficacy and effectiveness of blending turbulent pure hydrogen flames with four biofuel surrogates are tested on a coaxial needle spray burner. The flame appearance, flame luminosity, radiant heat flux, flame temperature, and spray characteristics of these biofuel/hydrogen flames are investigated by an experimental approach to understand the critical influencing factors in soot formation and the radiant intensity enhancement of hydrogen flames.

2. Methodology

2.1. Burner configuration

A coaxial needle spray burner was used to utilise the gas-assist atomisation for biofuel surrogates addition to the hydrogen-based flame. A dispensing needle with 300 mm length (L), 603 μm internal diameter (ID), and 908 μm outside diameter (OD) is located in the centre to supply the liquid biofuel surrogates. Hydrogen is issued from a concentrically mounted gas jet with ID = 6.1 mm as the carrier gas for gas-assist atomisation. The liquid and gaseous fuel jets are inserted in a stainless steel jet which supplies an air coflow. The schematic of the needle spray burner is shown in Fig. 2.

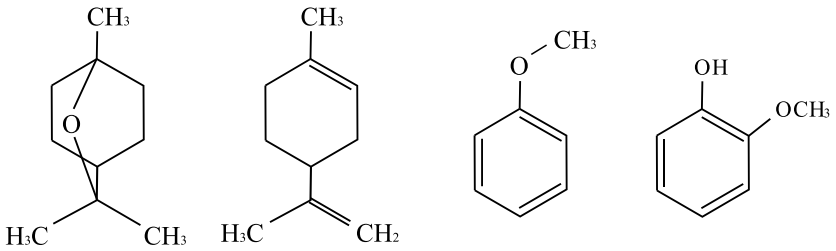

Fig. 1. Chemical structure of biofuel surrogates.

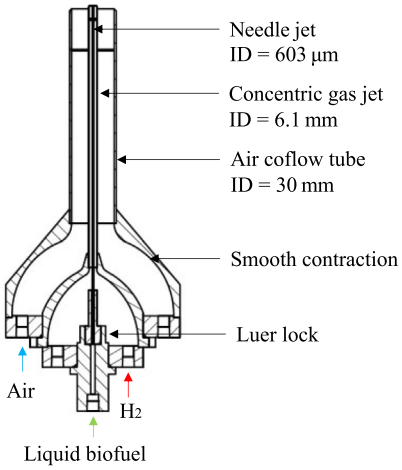

Fig. 2. Schematic of coaxial needle spray burner. The "ID" denotes the internal diameter.

2.2. Flame cases and test conditions

One of the major challenges for the gas-assist atomisation of biofuel additives is ensuring the ambient gas condition is able to generate sprays that can be completely consumed within the flame, while maximising the fuel-rich condition for soot formation. The bulk mean velocity of hydrogen was kept constant at $205\,\mathrm{m\,s^{-1}}$ to attain a bulk mean Reynolds number of 10,000, ensuring a turbulent flow regime in all flow cases. The details of the flame cases and the corresponding flame codes are shown in Table 1. Turbulent nonpremixed hydrogen-based flames were blended with liquid biofuel surrogates by gas-assist atomisation with different concentrations. The flow rates of the four biofuel surrogates were kept constant across the flame cases with a concentration equivalent to 0%, 0.1%, 0.2%, and 0.3% based on the mole concentration of H_2, respectively. In addition, the carbon flow rate across different biofuel surrogates at the same concentration was kept constant to achieve an equivalent carbon flux. The ambient temperature and pressure were 25°C and 1 atm, respectively.

The major non-dimensional influencing parameters for spray atomisation are calculated and presented in Table 1. The gas/liquid (g/l) momentum flux ratio (ψ_p), exit Weber number (We), gas/liquid bulk mean Reynolds number ratio (ψ_{Re}), and Ohnesorge number (Oh) are defined in Eqs. (1), (2), (3), and (4), respectively [33].

$$\psi_p = \frac{\rho_g U_g^2}{\rho_l U_l^2} \tag{1}$$

$$We = \frac{\rho_g (U_g - U_l)^2 D_l}{\sigma} \tag{2}$$

$$Re = \frac{\rho U L}{\mu} \tag{3}$$

$$Oh = \frac{\mu}{\sqrt{\rho \sigma L}} \tag{4}$$

where ρ denotes the density of the fluid, U is the bulk mean velocity, σ is the surface tension of the liquid, μ is the dynamic viscosity of the fluid, D_l is the initial liquid jet diameter, and L is the jet diameter of the fluid.

2.3. Experimental setup

Fig. 3 shows the schematic diagram of the experimental setup. As mentioned in Section 1, the risk of fire hazard may increase if the liquid droplets cannot react completely within the flame. Therefore, the coaxial needle spray burner was oriented horizontally in conjunction with a metal drip tray to control the potential escaped liquid droplets. For the selected flames, no escaped liquid droplet from the flame was observed in the experiment.

To capture the flame appearance and the resultant changes in the appearance due to the biofuel surrogate addition, a digital single-lens-reflex (DSLR) camera (Canon 6D) with a 50 mm focal length was used. The in-plane spatial resolution is 0.6 mm. The field of view (FOV) of the cropped image is 1411 mm × 644 mm (length × width). In the image post-processing, the photographs were transformed into greyscale to extract signal intensity from each pixel for quantitative flame luminosity analysis. The greyscale images were then binarised to obtain the flame area by counting the white pixels in the FOV of the cropped image.

To measure the global radiant heat flux of various biofuel surrogate-blended hydrogen flames, a heat flux sensor (Schmidt–Boelter gauge, Medtherm Corporation) was employed. The heat flux sensor is able to measure nominal radiation over the range of 5–200 $\mathrm{kW\,m^{-2}}$, with a full-field angle view of 150°. The heat flux sensor was located at the radial distance of 284 mm perpendicular to the centreline of the jet. The uncertainty calculated from the mean radiative heat flux data was within ±2%.

Soot formation and corresponding radiant heat flux have a close relationship with flame temperature [10]. In addition, the enthalpy of vapourisation in spray flames decreases the flame temperature, which in turn has an impact on the soot formation process. A Type R thermocouple with 0.2 mm diameter wire size and a 0.7 mm diameter bare-bead was employed to collect the mean flame temperature at the distance of 150 mm from the jet exit, focusing on the momentum-driven part of the flame and near-field of gas-assist atomisation. While a full axial profile of the temperature would have been useful, it was not practicable due to the horizontal nature of the flames. Nonetheless, the temperature data at $x = 150$ mm serves the purpose of relating the drop in gaseous temperature with the increase in thermal radiation from the flames and the enthalpy of vaporisation. The conclusions drawn from these measurements are carefully made to account for the fact that the measurements are made at one point in all flames. The flame temperature measurements were corrected for radiative heat loss from the thermocouple. The uncertainty of the mean flame temperature measurement was estimated to be ±6%.

Table 1
Details of flame cases and flame codes of the turbulent nonpremixed biofuel surrogates blended hydrogen flames, including mole fraction of additives based on the mole fraction of hydrogen (mol%), volumetric flow rate of biofuel surrogates (V_b), total heat input (Q), gas/liquid momentum flux ratio (ψ_{p_A}), bulk mean Weber number (We), bulk mean Reynolds number (Re), and Ohnesorge number (Oh). The flame codes and corresponding flame cases are as follows: "HU0" — unblended pure hydrogen flame; "HE" — H_2/Eucalyptol; "HL" — H_2/D-limonene; "HA" — H_2/Anisole; and "HG" — H_2/Guaiacol.

Flame code	mol%	V_b (mL/ min)	Q (kW)	ψ_{p_A}	We	Re	Oh
HU0	0.0	–	43.0	N/A	N/A	10,000	N/A
HL0.1	0.1	2	44.1	439	81	10,300	0.0073
HL0.2	0.2	3	45.1	110	81	10,700	0.0073
HL0.3	0.3	5	46.1	49	81	11,000	0.0073
HE0.1	0.1	2	44.2	375	34	10,400	0.0138
HE0.2	0.2	3	45.3	94	34	10,900	0.0138
HE0.3	0.3	5	46.5	42	34	11,000	0.0138
HG0.1	0.1	2	44.0	342	56	10,400	0.0385
HG0.2	0.2	3	44.9	85	56	11,000	0.0385
HG0.3	0.3	5	45.9	38	56	11,500	0.0385
HA0.1	0.1	2	43.9	404	60	10,300	0.0068
HA0.2	0.2	3	44.8	101	60	10,800	0.0068
HA0.3	0.3	5	45.7	45	60	11,000	0.0068

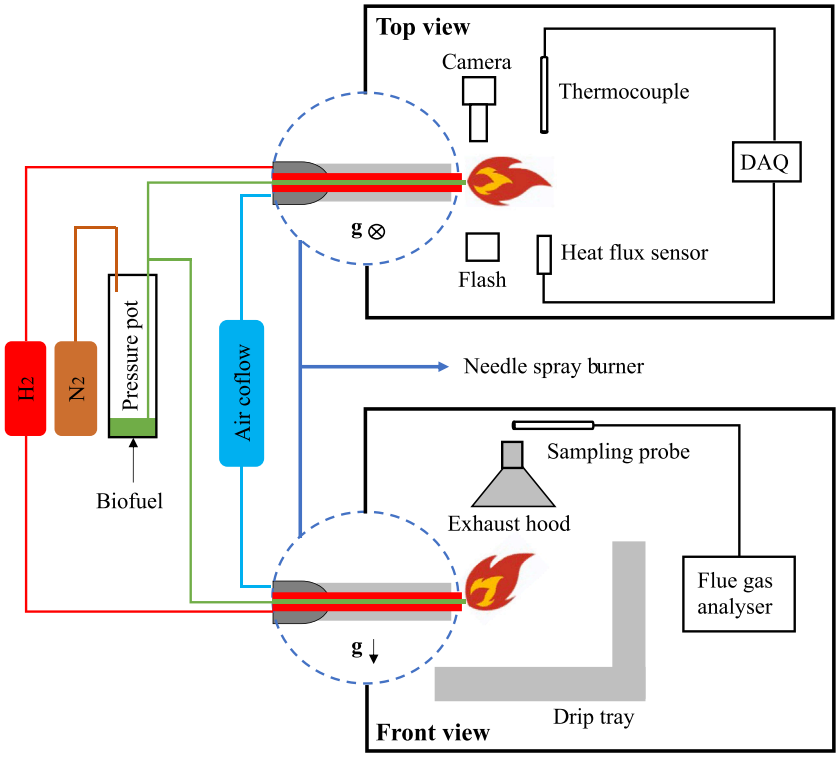

Fig. 3. Schematic of experimental setup. "DAQ" refers to the data acquisition systems. "**g**" indicates the direction of gravity.

To investigate the influence of spray characteristics of various biofuel surrogates generated by gas-assist atomisation, back-lit microscopic shadowgraph imaging was employed. This technique uses a light source to back-illuminate the objects from one side, and a detector to capture the light on the opposite side to the source. In this study, a DSLR camera (Canon 50D) was used as the detector to capture the light from the objects. A long-distance microscope (K_2 DistaMax Infinity) and a CF-2 objective were equipped with the DSLR camera for the magnification of the near-field spray structure. An electronic flash (Canon EL-1) was used as the illumination light source with a nominal flash duration of 10 μs to "freeze" the motion of the spray objects. The FOV and the depth of field (DOF) of the optical setup were 10 mm × 9 mm (length × width) and 3 mm, respectively. The in-plane spatial resolution was determined from the FOV divided by the image resolution (i.e. total pixels of the camera) as 3 μm.

2.4. Chemical analysis

In this study, numerical simulations were utilised to gain a deeper comprehension of the chemistry involved and the dominant reaction pathways responsible for polycyclic aromatic hydrocarbon (PAH) formation in biofuel-blended hydrogen flames. The simulations were conducted using the opposed-flow non-premixed (OPPDIF) flame model in Chemkin Pro v19.2. The OPPDIF model, commonly combined with experimental methods, allows for an investigation of flame behaviour and chemical kinetics in jet flames [34,35].

The chemical kinetic mechanism employed in this research was developed by the CRECK Modelling Group specifically for modelling soot formation [36,37]. It consists of 24,501 reactions and 497 species related to the combustion of hydrocarbons ranging from C_1 to C_{16}.

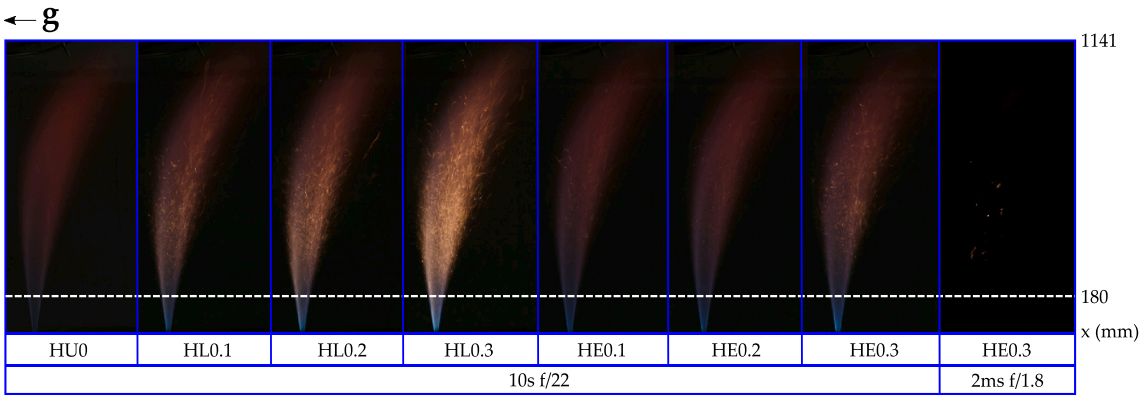

(a) Flame appearance of spray essential oil surrogates blended hydrogen flames

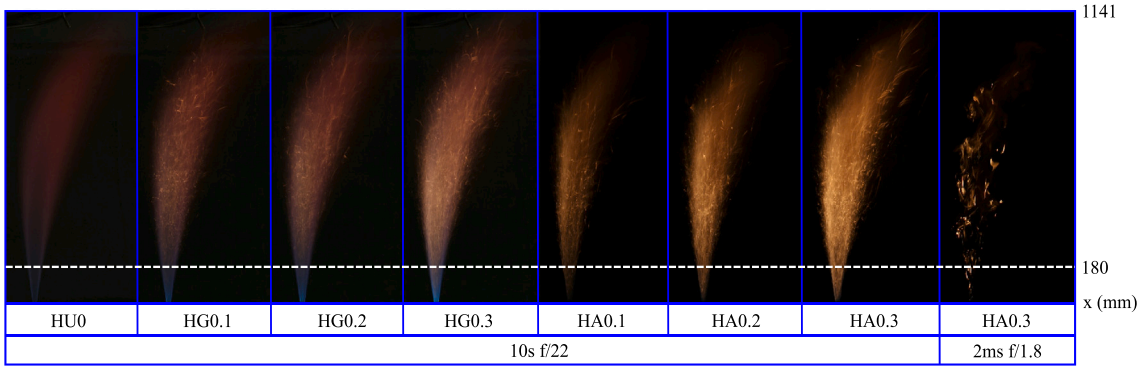

(b) Flame appearance of spray bio-oil surrogates blended hydrogen flames

Fig. 4. Flame appearance of spray essential oil surrogates blended 4(a) and bio-oil surrogates blended 4(b) hydrogen flames. The flames were established on the horizontally oriented needle spray burner described in Section 2.1. "**g**" indicates the direction of gravity relative to the flame. The long-exposure (10 s) and short-exposure (2 ms) photographs were taken at ISO-100.

However, the current study only considered the presence of anisole and guaiacol in the chemical kinetics modelling. To the best of the authors' knowledge, a comprehensive chemical kinetics mechanism that includes soot precursors is not available for essential oil surrogates—eucalyptol and D-limonene. The concentrations of guaiacol and anisole were varied while keeping the H_2 concentration fixed to simulate different experimental cases. The fuel and oxidant inlet velocities were adjusted to maintain similar momentum conditions. To predict soot formation and the corresponding thermal radiation in the biofuel-blended hydrogen flames, the Chemkin simulation focused on analysing naphthalene ($C_{10}H_8$, hereafter referred to as A_2). Naphthalene is commonly employed in numerical studies as a key intermediate in the formation of large PAHs to investigate soot formation [1,38,39].

3. Results and discussion

3.1. Flame appearance

The flame appearance of the spray biofuel surrogate blended hydrogen flames is compared with the unblended hydrogen flame, shown in Fig. 4. The spray essential oil surrogates (i.e. D-limonene and eucalyptol) and bio-oil surrogates (i.e. guaiacol and anisole) blended hydrogen flames are presented in Fig. 4(a) and Fig. 4(b), respectively. The long-exposure (10 s) photographs illustrate the mean characteristics of the biofuel surrogate blended hydrogen flames. Additional short-exposure photographs (2 ms) of eucalyptol and anisole blended hydrogen flames capture the instantaneous soot distribution in the flame envelope.

The unblended hydrogen flame (HU0) is dominated by red colouration due to the presence of water vapour as the major combustion product of hydrogen. It is the least luminous flame presented in Fig. 4. With the addition of 0.1–0.3% biofuel surrogates, the visibility of the unblended hydrogen flame is improved. As the biofuel surrogates are added to the flame, enhanced blue colouration appears near the jet exit (axial distance x = 0–180 mm from the jet exit) in contrast to the nearly invisible region in the unblended hydrogen flame. The enhanced blue colouration is ascribed to the formation of carbonaceous radicals—HCO^*, C_2^*, CH^*, and CO_2^* by the biofuel blending [1]. The red colouration from the middle to the tip of the unblended hydrogen flame is transformed to yellow, which is a typical indication of soot formation, as the 0.1, 0.2, and 0.3 mol% biofuel surrogates are added. Soot particles are essentially carbon clusters that are incandescent at high temperatures. As they form within the flame, they absorb thermal energy and emit light through black body radiation. The emitted light tends to be in the visible spectrum and the colour tends towards yellow. Hence the transition of the flame colouration from red (the soot-free hydrogen flame) to yellow indicates soot formation is enhanced in the flame through biofuel surrogate addition.

A clear shift to yellow colouration is achieved by the gas-assist atomisation of the biofuel additives. In contrast, it has been reported that adding 0.2–1 mol% biofuel surrogates by prevapourisation or ultrasonic atomisation enhances the blue colouration due to promoted formation of carbonaceous radicals, but the transition to yellow colouration was not observed [10]. The dominant source of flame luminosity is shifted from gaseous species to soot particulates in these sooting gas-assist atomised biofuel surrogate/hydrogen flames. The promoted soot loading in the gas-assist atomised biofuel surrogate/hydrogen flames indicates that the alternation of the introduction method benefits the soot formation. From the direct observation of the photographs, the yellow colouration transformation is the most intensive in anisole/hydrogen flames. The region near the jet exit is occupied by yellow colouration, indicating an early formation of soot particulates in anisole/hydrogen flames. The eucalyptol/hydrogen flame illustrates the

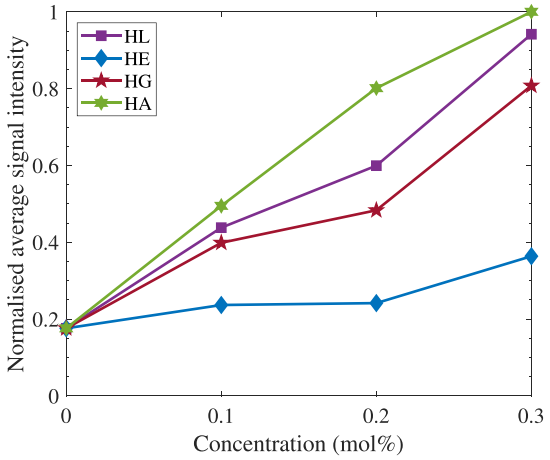

Fig. 5. Flame luminosity indicated by the average signal intensity from photographs of spray biofuel surrogate blended H_2 flames described in Table 1. The hydrogen flames contain either limonene (HL), eucalyptol (HE), guaiacol (HG), or anisole (HA). The average signal intensity is calculated by the summation of each pixel signal intensity and the flame area obtained from the binarised image. The average signal intensity is normalised to the peak signal intensity of 0.3 mol% anisole-blended H_2 flame.

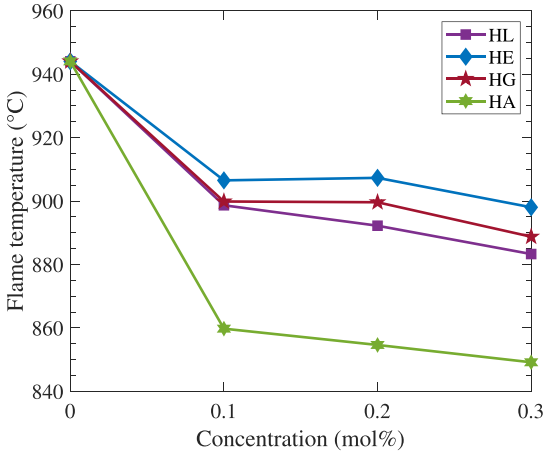

Fig. 6. Flame temperature of spray biofuel surrogate blended H_2 flames measured at axial distance x = 150 mm from the jet exit on centreline. The hydrogen flames contain either limonene (HL), eucalyptol (HE), guaiacol (HG), or anisole (HA). The flame temperature is corrected for radiative heat loss from the thermocouple.

least enhancement in luminosity and soot formation among all biofuel surrogates.

The short-exposure photograph of anisole/hydrogen shows that soot particulates evidently cluster from the jet exit to the flame tip, whereas the soot can be barely seen in eucalyptol/hydrogen flames at the same camera settings. The soot clusters in anisole/hydrogen flames are ascribed to the local fuel-rich region created by large liquid fuel droplets from gas-assist atomisation, which will be further demonstrated by microscopic shadowgraphs in Section 3.4. The larger droplets generated from gas-assist atomisation benefit soot formation and corresponding luminosity enhancement by creating more intensive local fuel-rich conditions.

The average signal intensity extracted from the photographs shown in Fig. 5 can present quantitative information on the luminosity of the flames. The average signal intensity is calculated by the summation of each pixel signal intensity in the FOV of the cropped image and the flame area obtained from the binarised image. The average signal intensity is normalised to the average signal intensity of 0.3 mol% anisole/hydrogen flame. The average signal intensity increases with the addition of gas-assist atomised biofuel surrogates, indicating that the flame luminosity of the hydrogen-based flame is enhanced by the addition of biofuel surrogates. The highest luminosity is found in the 0.3 mol% spray anisole/hydrogen flame, which is five times more luminous than the unblended hydrogen flame. The smallest luminosity increase of the unblended hydrogen flame is also 30% from blending 0.1 mol% spray eucalyptol/hydrogen flame. The luminosity enhancement of the unblended hydrogen flame is enhanced by 400% by the addition of 0.2 mol% gas-assist atomised anisole, whereas the 0.2 mol% prevapourised and ultrasonically atomised anisole only increases the luminosity by 200% [10]. The effectiveness of biofuel surrogates in hydrogen flame luminosity enhancement follows the trend as anisole > D-limonene > guaiacol > eucalyptol. The luminosity of these sooting gas-assist atomised biofuel/hydrogen flames is primarily contributed by the incandescence from soot particulates formed in the flame. Anisole produces the most soot among the biofuel surrogates, thus it has the most luminosity enhancement. The effect of functional groups will be discussed together with the radiant fraction results in Section 3.3. The average signal intensity extracted from the photographs further provides quantitative evidence to support the effectiveness of luminosity enhancement of biofuel blending, in addition to the direct observation of the photographs.

3.2. Flame temperature

The flame temperature measured at x = 150 mm (axial distance from the jet exit on centreline) of the gas-assist atomised biofuel surrogate/hydrogen flame as a function of additive's concentration is presented in Fig. 6. The flame temperature shows a decreasing trend with the addition of biofuel additives. The unblended hydrogen flame has a flame temperature of 945°C. The 0.3 mol% anisole/hydrogen flame exhibits the lowest flame temperature at 850°C. The flame temperature drop as a result of spray biofuel addition is up to 95°C. The flame temperature of biofuel surrogate blended hydrogen flames follows the trend from high to low as eucalyptol > guaiacol > limonene > anisole. The phenomenon of flame temperature drop with the spray biofuel addition is ascribed to the following factors: (1) the lower flame temperature of the biofuel surrogates; (2) the enthalpy of vapourisation; and (3) the radiative heat loss from the promoted soot loading in the blended flames. The larger droplets formed by the gas-assist atomisation lead to a greater enthalpy of vapourisation.

It is observed from Figs. 4–6 that the luminosity enhancement of the biofuel surrogates shows a reverse trend to the flame temperature drop. Anisole blends exhibit the largest luminosity enhancement while displaying the most significant flame temperature drop. This phenomenon implies that the radiative heat loss becomes a major factor of the flame temperature drop in these sooting blended hydrogen flames. As discussed in Section 3.1, sooting biofuel surrogate/hydrogen flames are achieved by the gas-assist atomisation such that the presence of the soot particulates is the major contribution to flame luminosity enhancement. As the soot formation is promoted with the biofuel surrogate addition, the fraction of radiative heat transfer is increased in the total heat output of the fuel mixture correspondingly, leading to the flame temperature decreases. Therefore, the biofuel surrogate that produces more soot particulates tends to have a larger flame temperature drop. It is also observed that the centreline temperature drop in these sooting gas-assist atomised biofuel surrogate/hydrogen flames is more significant than that in non-sooting ultrasonically atomised biofuel surrogate/hydrogen flames [9,10]. Despite the factor of the enthalpy of vapourisation in both flames, the additional radiative heat loss from sooting gas-assist atomised biofuel/hydrogen flames may cause the larger flame temperature drop. The radiant fraction presented in the following Section 3.3 will further support this hypothesis.

3.3. Radiant heat flux

To investigate the radiant heat flux enhancement by the addition of gas-assist atomised biofuel surrogates, a radiant fraction is calculated based on the global radiant heat flux data measured by the heat flux sensor. The radiant fraction is calculated using Eq. (5) [40]:

$$\chi_r = \frac{\dot{Q}_r}{\dot{Q}_F} = \frac{2 \cdot \pi \cdot \left(\int_{R_0}^{R} r \cdot \dot{q}''(r) \cdot dr + R \cdot \int_0^{\infty} \dot{q}''(z) \cdot dz \right)}{\dot{m} \times LHV} \quad (5)$$

where χ_r denotes the radiant fraction as the fraction of radiated heat $\dot{Q}_r$ (kW) normalised by the total heat input $\dot{Q}_F$ (kW) of the flame. The radiated heat ($\dot{Q}_r$) is acquired by the heat flux transducer, which is the summation of the axial (z) and radial (r) radiant heat flux ($\dot{q}''$). The radial distance between the heat flux sensor and the centre of the jet exit R and the flame front R_0 are considered in this equation. LHV and $\dot{m}$ denote the lower heating value and the mass flow rate of the fuel, respectively.

Fig. 7(a) presents the global radiant fraction of the unblended and gas-assist atomised biofuel surrogate/hydrogen flames as a function of the biofuel surrogates' concentration. All global radiant fractions of the blended hydrogen flame increase with the addition of the biofuel surrogates. The effectiveness of the biofuel surrogates in radiant fraction enhancement ranks from significant to mild as: anisole > limonene > eucalyptol > guaiacol. The largest radiant fraction enhancement of an unblended hydrogen flame is from the addition of 0.3 mol% anisole by 15%. The smallest increase in the radiant fraction of an unblended hydrogen flame is 2%, from the addition of 0.1% guaiacol. Both anisole and guaiacol have a methoxy group (-OCH_3) while guaiacol possesses an additional hydroxyl group (-OH) in the ortho position of the methoxy function. The decomposition of anisole and guaiacol initiates at the weakest O-C chemical bond in the methoxy group with bond dissociation enthalpy (BDE) of 243 kJ mol^{-1} (guaiacol) and 264 kJ mol^{-1} (anisole), respectively [30,41]. The loss of methyl group followed by ipso-additions on guaiacol forms pyrocatechol as the primary product of the guaiacol reaction. Pyrocatechol is comprised of two hydroxyl groups which are more readily accessible to react with soot and PAHs to promote soot oxidation [42]. In addition, the BDEs of the C-H bond in the aromatic ring of guaiacol (481–490 kJ mol^{-1}) are higher than that in anisole (471–476 kJ mol^{-1}), making the aromatic ring in guaiacol less reactive [30,43]. The formation of naphthalene—a critical intermediate in soot formation, has been detected in both pyrolysis and oxidation of anisole but only detected in the oxidation of guaiacol [30]. Compared with bio-oil surrogates, D-limonene, and eucalyptol are less effective than anisole on radiant fraction enhancement due to the higher unsaturation degree of aromatic structures, and the lowest BDE of the C-H bond in the allylic group of D-limonene (371 kJ mol^{-1}) is still much higher than that in anisole [44]. The minor effectiveness of guaiacol on radiant fraction enhancement compared with the essential oil surrogates may imply that the effect of the additional hydroxyl group in guaiacol on promoting PAH oxidation overwhelms the advantages of aromatic structures in PAH formation, resulting in a lower global radiant fraction.

The rate of production (ROP) of naphthalene (A_2) from the numerical simulation of guaiacol and anisole blended hydrogen flames, shown in Fig. 7(b), further supports the observation from the experimental results that anisole tends to have higher A_2 ROP than guaiacol hence larger radiant fraction enhancement. The A_2 ROP in the 0.3 mol% anisole-blended hydrogen flame is up to seven times greater than that in 0.3 mol% guaiacol-blended hydrogen flame. Figs. 8(a) and 8(b) illustrate six dominant chemical reaction pathways of A_2 formation in anisole/hydrogen and guaiacol/hydrogen flames, respectively. The results show that $H_2 + C_{10}H_7 \rightleftharpoons H + A_2$ is the most dominant chemical reaction in forming A_2 in both anisole/hydrogen and guaiacol/hydrogen flames, followed by the reverse reactions of $H_2 + A_2 \rightleftharpoons H + C_{10}H_7$, and $H + A_2 \rightleftharpoons 0.5 \cdot C_{10}H_7 + 0.5 \cdot$Tetralin. The similar dominant chemical reaction pathways of A_2 formation found in anisole and guaiacol suggest similar pyrolysis and reaction processes. The reaction initiates at the weakest O-C bond of the methoxy group in both anisole and guaiacol. The PAH formation in these two aromatic fuels is mainly attributed to H-abstractions, which is consistent with the kinetic studies in the literature [30,45]. Since guaiacol has a more stable aromatic structure with higher BDEs due to the presence of the additional hydroxyl group compared with anisole, although the dominant reactions are similar, the ROP of A_2 formation is significantly lower.

Table 2
Comparison of the effectiveness of radiant fraction enhancement from adding 0.2 mol% biofuel surrogates via prevapourisation, ultrasonic atomisation, and gas-assist atomisation. "PV" denotes prevapourisation, "UA" is ultrasonic atomisation, and "GA" is gas-assist atomisation. The results of the prevapourised and ultrasonic spray biofuel surrogate/hydrogen flames are from previous research [9,10]. The results from the gas-assist atomised biofuel surrogate/hydrogen flames are obtained in this study.

Introduction methods	PV	UA	GA
HE0.2	2%	4%	7%
HL0.2	6%	7%	9%
HA0.2	9%	10%	13%

Table 2 presents the comparison of the effectiveness of radiant fraction enhancement from adding 0.2 mol% biofuel surrogates via prevapourisation, ultrasonic atomisation, and gas-assist atomisation. It has been reported that adding prevapourised and ultrasonically atomised 0.2 mol% anisole enhanced the radiant fraction of unblended hydrogen flame by 9% and 10%, respectively, less effective than 13% enhancement of radiant fraction from adding 0.2 mol% anisole by gas-assist atomisation [9,10]. This is because in these sooting biofuel surrogate blended hydrogen flames, the radiant heat flux is primarily due to the blackbody radiation from soot particulates in the flame with minor contributions from the gaseous species such as CO_2 and water vapour. In contrast, the primary source of the radiant heat flux in prevapourised biofuel blended hydrogen flames is dominated by gaseous species. Given that radiant heat flux from soot particulates is much stronger than gaseous species, adding biofuel surrogates by gas-assist atomisation is more effective than the methods of prevapourisation and ultrasonic atomisation [46]. This trend agrees with the luminosity enhancement discussed in Section 3.1.

Soot formation, flame temperature, and radiant heat flux have complex interactions with each other. For a constant soot loading, higher flame temperature results in higher radiant heat flux because blackbody radiation has a quartic relationship with the temperature ($Q_r \propto T^4$). Hence, mild variation in flame temperature has a significant influence on the radiant heat flux. However, the higher temperature provides energy for soot oxidation and facilitates the soot oxidation rate, leading to a reduction in soot particulate which is the essential source of the blackbody radiation.

3.4. Microscopic shadowgraphy

The near-field spray characteristics are identified by the microscopic shadowgraph imaging as five major structures: (**A**) liquid core, (**B**) wave structure, (**C**) irregular object, (**D**) ligament, and (**E**) droplet. The liquid core (**A**) and wave structure (**B**) characterise the intact liquid stream as it is ejected from the jet. The subsequent formation of fragments **C**, **D**, and **E** may be classified by their aspect ratio (AR), characteristic major length (ℓ_{max}), and initial liquid jet diameter (D_l) as follows [26,47–51]:

- Droplets ($\ell_{max} < D_l$ and AR < 3).
- Ligaments (AR > 3).
- Irregular objects (AR > 3, $\ell_{max} > D_l$).

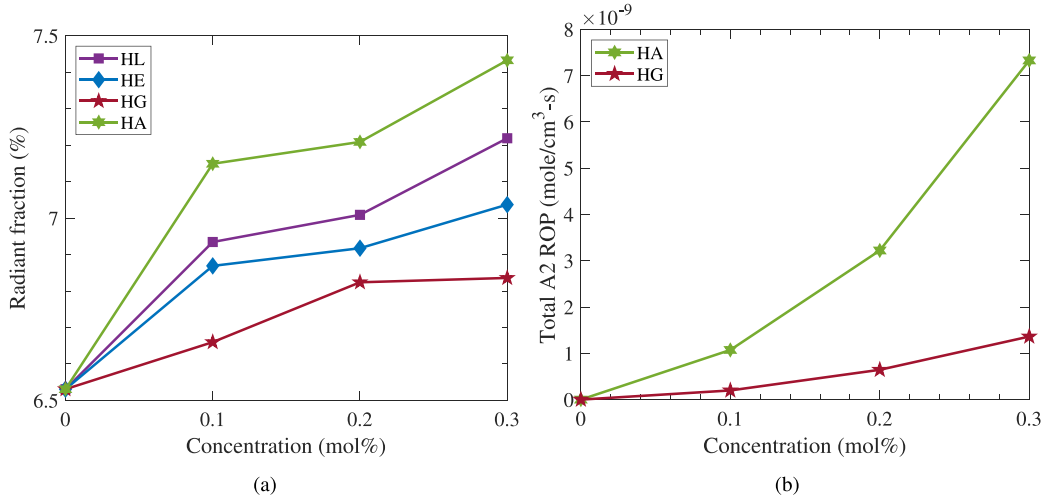

Fig. 7. 7(a) Global radiant fraction measured from spray biofuel surrogate blended H_2 flames described in Table 1. 7(b) The rate of production (ROP) of naphthalene (A_2) from numerical simulation of guaiacol and anisole blended H_2 flames. The hydrogen flames contain either limonene (HL), eucalyptol (HE), guaiacol (HG), or anisole (HA).

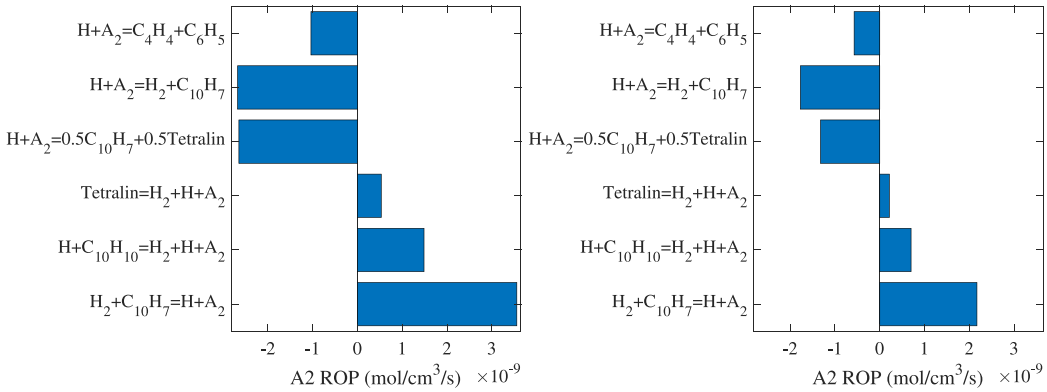

Fig. 8. Dominant chemical reaction pathways of naphthalene (A_2) formation in anisole/hydrogen 8(a) and guaiacol/hydrogen 8(b) flames described in Table 1.

where AR is the aspect ratio, ℓ_{max} is the characteristic major length, and D_l is the initial liquid jet diameter.

The representative microscopic shadowgraphs of the near-field spray characteristics of the biofuel surrogate/hydrogen flames are shown in Fig. 9. From the direct observation from the shadowgraphs, guaiacol, and eucalyptol sprays appear to display different overall spray characteristics compared with D-limonene and anisole sprays. Guaiacol and eucalyptol sprays exhibit more dispersed spray than D-limonene and anisole sprays, indicating a finer spray. A relatively larger number of droplets are present in the near-field region of the spray in D-limonene and anisole flames in contrast to very limited droplets generated in eucalyptol and guaiacol sprays. The liquid core of the eucalyptol spray is evidently more elongated than the D-limonene and anisole sprays. The extent of the liquid core elongation is even more significant in guaiacol sprays. These observations are ascribed to the different physical properties of eucalyptol and guaiacol that they have higher viscosity and surface tension than D-limonene and anisole, which in turn have a significant impact on the spray characteristics. The dynamic viscosity of eucalyptol is 2.6 mPa s whereas the dynamic viscosity of D-limonene and anisole is less than 1 mPa s [21,52,53]. Guaiacol, the representative pattern of lignin, has a dynamic viscosity of 6.1 mPa s, more than six times greater than D-limonene and anisole [54,55]. Similar to the viscosity difference, the surface tensions of guaiacol 37 mN m^{-1} and eucalyptol 62 mN m^{-1} are higher than D-limonene (26 mN m^{-1}) and anisole (35 mN m^{-1}) [56–58].

The distinct physical properties of the liquid fuel lead to a large difference in exit Weber number and Ohnesorge number, which are critical non-dimensional influencing parameters for spray characteristics. The Weber number indicates the relationship between the disruptive hydrodynamic force—inertia force and the stablising force—surface tension in fluid dynamics. The Ohnesorge number reflects the effect of viscosity on the tendency of the droplet breakup. A larger Ohnesorge number requires a larger critical Weber number for liquid stream breakup which is defined as the value at which droplet breakup occurs. It is seen in Table 1 that the exit Weber number and Ohnesorge number of the biofuel surrogate blended flames are insensitive to the liquid fuel concentration because the liquid flow rate is very low compared with the gas flow rate. Since the density of the liquid fuel is similar (840–1100 kg m^{-3}), the difference in these two parameters is mainly from their viscosity and surface tension. The exit Weber number of D-limonene and anisole are larger than guaiacol and eucalyptol, indicating that the inertia force tends to overcome the cohesion force more easily in these fluids hence resulting in more intensive liquid stream breakup. The Oh of guaiacol (0.0385) is the largest followed by eucalyptol (0.0138), whereas D-limonene and anisole have similar smaller values of $Oh \approx 0.007$. A larger value of Oh implies that the effect of viscosity has a greater impact on the dispersion of droplets that they tend to cluster together. These analyses of the physical properties and influencing parameters explain the direct observations from the microscopic shadowgraphs.

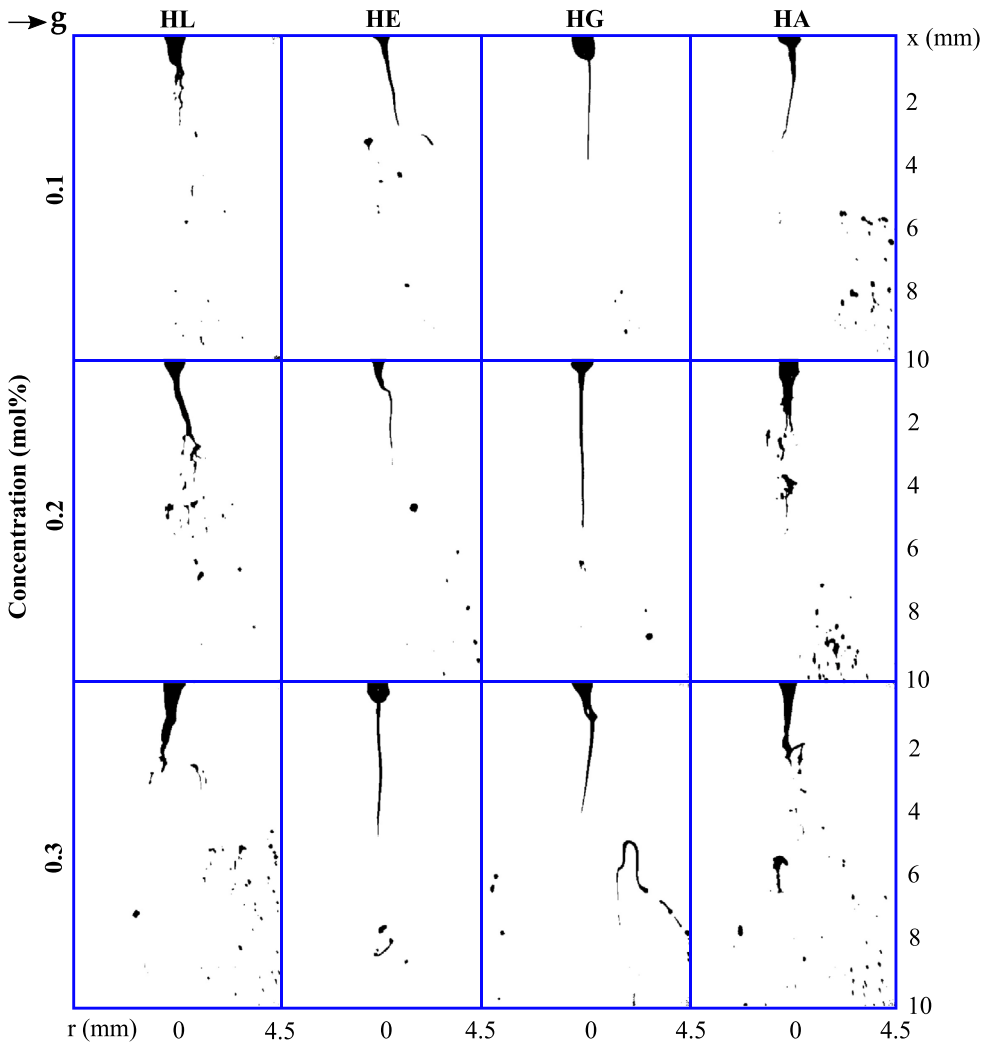

Fig. 9. Representative microscopic shadowgraphs for the near-field (x = 0–10 mm) spray characteristics of biofuel surrogate blended H_2 flames described in Table 1. "**g**" indicates the direction of gravity relative to the flame.

The key spray characteristics including breakup length, the characteristic major length (ℓ_{max}) of droplets, and the area fraction (A_S/A_T) of the spray objects occupied area to the total area (FOV) are extracted from the microscopic shadowgraphs to study the sprays of different biofuel surrogates. The breakup length, the characteristic major length (ℓ_{max}) of droplets and ligaments, and the area fraction (A_S/A_T) of the biofuel surrogate sprays as a function of biofuel surrogate concentration, gas/liquid momentum flux ratio (ψ_p), gas/liquid Reynolds number ratio (ψ_{Re}), and exit Weber number (We) are presented in Figs. 10, 11, and 12, respectively.

Fig. 10 shows that for the same biofuel surrogate, the breakup length of the gas-assist biofuel spray increases with the liquid loading and decreases with the gas/liquid momentum flux ratio (ψ_p). Larger ψ_p and ψ_{Re} values induce a higher level of instabilities on the gas/liquid interface and turbulence of the flows, leading to a more intense primary breakup of the liquid stream. A larger breakup length value is an indication of a coarser spray. It is observed that the gas/liquid momentum flux ratio (ψ_p) is not suitable for predicting breakup length across various liquid fuels since the breakup length varies across different liquid fuels at the same ψ_p. This means that other factors such as viscosity and surface tension may play a non-negligible role in the variation of breakup length. Guaiacol sprays display the largest breakup length followed by eucalyptol sprays. The breakup lengths of D-limonene and anisole are similar and smaller than eucalyptol sprays. This trend of breakup length is consistent with the order of the fuel viscosity—guaiacol > eucalyptol > D-limonene ≈ anisole, implying that the viscosity of the liquid fuel may have a significant impact on the breakup length of the gas-assist spray. In the guaiacol and eucalyptol sprays, the liquid cores are elongated as a result of higher viscosity and surface tension acting against the disruptive force from the instabilities on the surface. The resistance of the higher viscosity to the motion of the flow keeps the liquid stream propagating in the direction of the initial momentum rather than spreading into a wide angle of direction. The elongated liquid core eventually breaks at a weak point into ligaments with large characteristic major lengths and aspect ratios rather than directly into droplets. Hence more ligament structures with larger ℓ_{max} are observed in guaiacol and eucalyptol sprays in contrast to D-limonene and anisole sprays.

The characteristic major length of droplets, shown in Fig. 11, increases with the liquid loading and decreases with ψ_p, ψ_{Re}, and We. The characteristic major length of droplets in the gas-assist spray flames ranges from 0.08–0.34 mm. Dissimilar to the breakup length trend, eucalyptol sprays generate the largest droplets followed by guaiacol sprays, anisole sprays, and D-limonene sprays. The order of the droplets ℓ_{max} is the reverse order of the We in Table 1 as eucalyptol > guaiacol > anisole > D-limonene, indicating that We is the dominant parameter for predicting the droplet size in gas-assist sprays. In conjunction with the observations of the breakup length, the liquid streams of D-limonene and anisole break up early into droplets while the liquid stream undergoes an elongation and then breaks up into ligaments. The number of

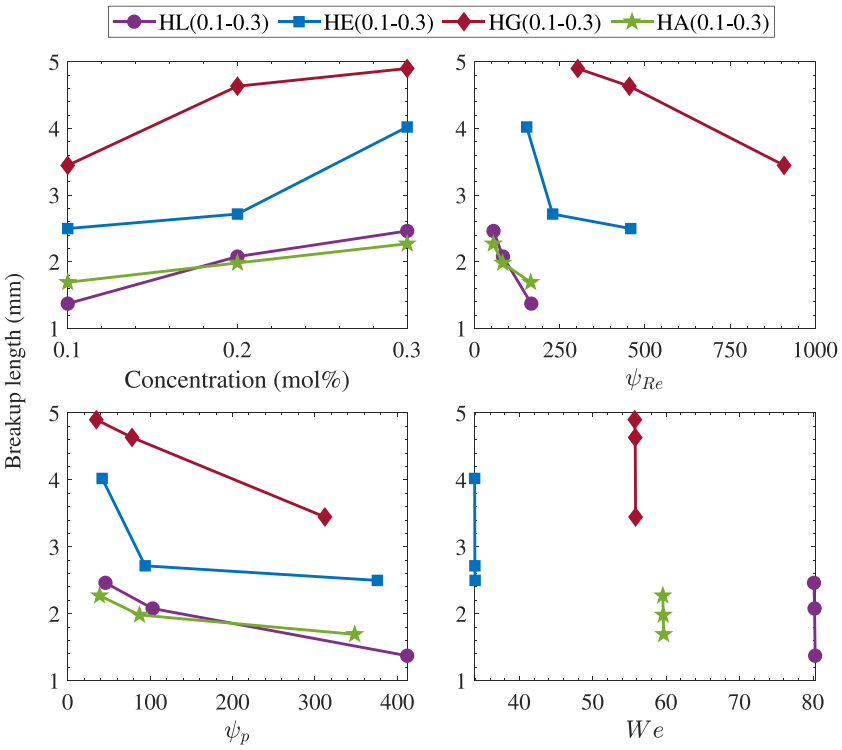

Fig. 10. Breakup length of the gas-assist biofuel surrogate sprays as a function of biofuel concentration, gas/liquid momentum flux ratio (ψ_p), gas/liquid Reynolds number ratio (ψ_{Re}), and exit Weber number (We).

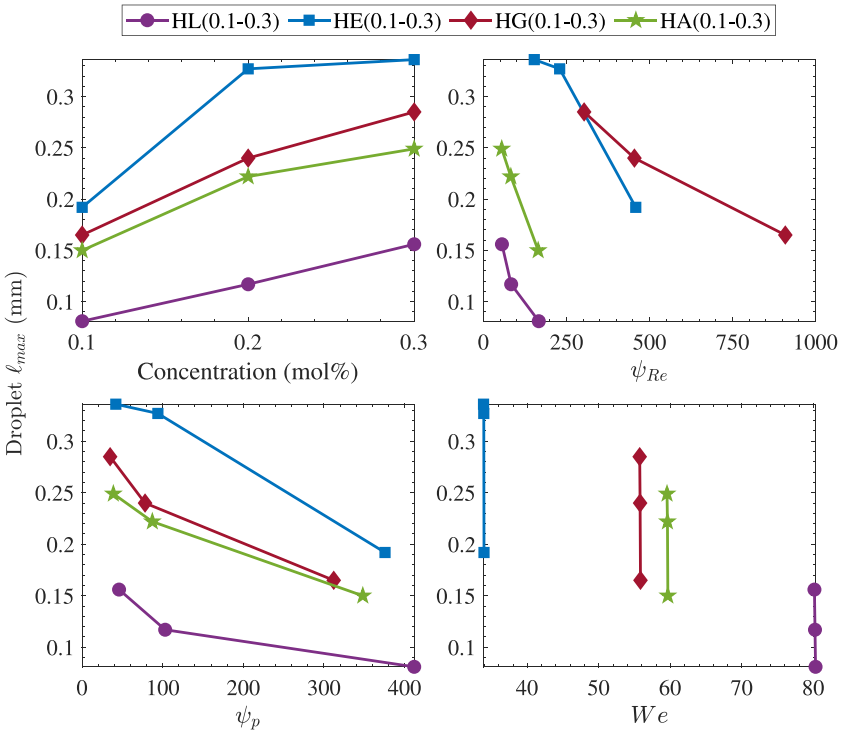

Fig. 11. Droplet characteristic major length (ℓ_{max}) of the gas-assist biofuel surrogate sprays as a function of biofuel concentration, gas/liquid momentum flux ratio (ψ_p), gas/liquid Reynolds number ratio (ψ_{Re}), and exit Weber number (We).

droplets in D-limonene and anisole sprays is more than that in guaiacol and eucalyptol sprays. The dispersion of the spray objects can be further investigated by the area fraction results.

Fig. 12 displays the area fraction of the biofuel surrogate spray flames. The area fraction is calculated by the area occupied by the spray objects and the FOV. For the same type of biofuel surrogate, the area fraction increases with the liquid loading and decreases with ψ_p and ψ_{Re}. It is interesting that the ψ_{Re} appears to dominate in describing the area fraction. The area fraction of these biofuel spray flames is mainly influenced by two factors: (i) surface area growth as a result of the

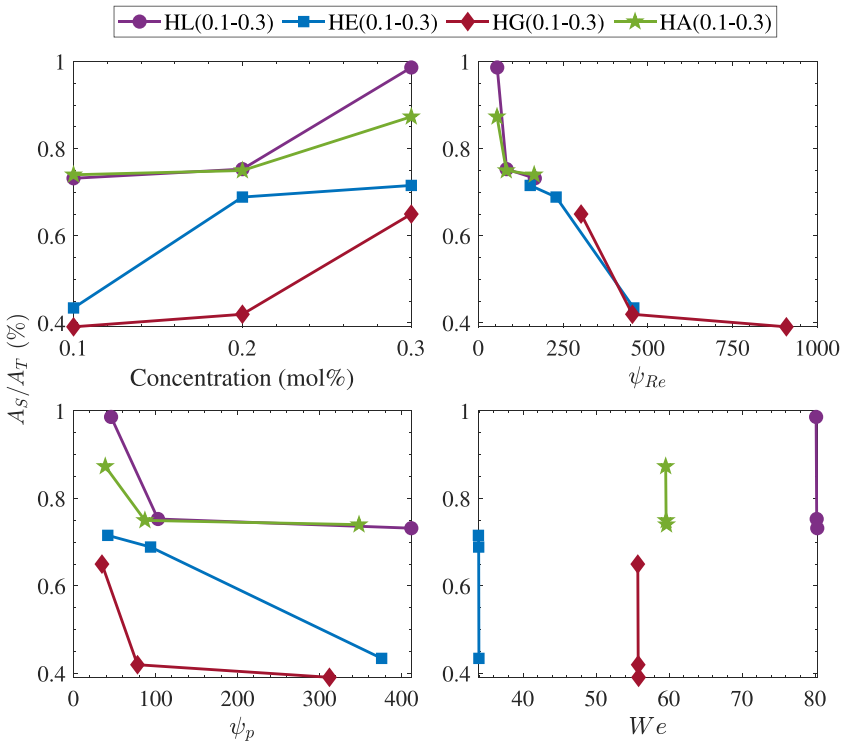

Fig. 12. Area fraction (A_S/A_T%) of the gas-assist biofuel surrogate sprays as a function of biofuel concentration, gas/liquid momentum flux ratio (ψ_p), gas/liquid Reynolds number ratio (ψ_{Re}), and exit Weber number (We).

primary and secondary breakup; and (ii) evaporation rate of the liquid in the spray flame. The guaiacol spray has the lowest area fraction among all biofuel surrogates, which agrees with the observations of breakup length and droplet size results, appearing to be the most coarse spray. The area fractions of the biofuel surrogates follow the order from low to high as guaiacol < eucalyptol < anisole < D-limonene, which is the opposite order of the Ohnesorge number. The area fraction analysis provides evidence to further support that liquid fuel with higher viscosity and surface tension tends to have lower dispersion and coarser sprays than that with lower viscosity and surface tension.

The results of spray characteristics provide evidence to analyse the more effective flame luminosity and radiant fraction enhancement found in gas-assist atomised biofuel/hydrogen flames, compared with prevapourised and ultrasonically atomised biofuel/hydrogen flames. The droplet size formed by gas-assist atomisation is found between 0.15–0.34 mm, much larger than the droplet size generated by ultrasonic atomisation at 0.03 mm (specified by the manufacturer) [10]. The presence of larger droplets in gas-assist atomised biofuel/hydrogen flames creates even more extreme fuel-rich conditions which further favours soot formation. In addition, the ultrasonically atomised droplets are entrained by hydrogen upstream of the jet exit and have an earlier and more homogeneous mixing with gaseous fuels, compared with less dispersion of liquid droplets and later mixing downstream of the jet exit in gas-assist atomisation. Therefore, the mixing of liquid fuel droplets and the local OH radicals from the reaction of hydrogen in gas-assist atomised biofuel/hydrogen flames is less homogeneous, again resulting in localised fuel-rich conditions.

4. Conclusions

The effect of adding biofuel surrogates to turbulent nonpremixed pure hydrogen flames by gas-assist atomisation on the flame characteristics was investigated. The flame appearance, flame luminosity, flame temperature, radiant fraction, and near-field spray characteristics of essential oil surrogates (eucalyptol and D-limonene) and bio-oil surrogates (guaiacol and anisole) blended hydrogen flames were measured by experimental approaches. The key findings of this study are summarised as follows:

1. Thermal radiation of hydrogen flames was increased by blending biofuel surrogates in a coaxial spray burner by taking advantage of the gas-assist atomisation. A clear transition of flame colouration from blue/red to yellow was observed with the addition of 0.1–0.3 mol% biofuel surrogates.
2. The flame luminosity and the radiant fraction of the unblended hydrogen flame were increased by 30%–500% and 2%–15%, respectively, from the addition of 0.1–0.3 mol% biofuel surrogates, demonstrating that blending the biofuel surrogates by gas-assist atomisation is more effective than prevapourisation and ultrasonic atomisation.
3. The flame temperature measured at $x = 150$ mm on the centre axis of the gas-assist atomised biofuel surrogate/hydrogen flames dropped evidently due to the enthalpy of vapourisation and the promoted radiative heat loss from the enhanced soot formation.
4. The viscosity and surface tension of the liquid biofuel surrogates and the resultant variation in Weber number and Ohnesorge number impact the near-field spray characteristics. The droplets' characteristic major length of biofuel surrogate sprays is dominated by exit Weber number, following the reverse order of We as eucalyptol > guaiacol > anisole > D-limonene. The area fraction of the biofuel surrogate sprays from low to high follows the order of guaiacol < eucalyptol < anisole < D-limonene, which is the reverse order of the Ohnesorge number. Guaiacol and eucalyptol sprays, which have higher viscosity and surface tension tend to generate coarser sprays than D-limonene and anisole.
5. Guaiacol, as a representative of the lignin pattern, is less effective than anisole, D-limonene, and eucalyptol in radiant fraction enhancement due to (i) the hydroxyl group promotes PAH oxidation; (ii) higher BDE of the aromatic ring makes guaiacol

less reactive; and (iii) a coarser spay, i.e. larger breakup length, droplet size, ligament size, and less dispersed spray objects generated by the gas-assist atomisation compared with other biofuel surrogates tested.

CRediT authorship contribution statement

Yilong Yin: Writing – original draft, Software, Methodology, Investigation, Formal analysis, Data curation, Conceptualization. **Paul R. Medwell:** Writing – review & editing, Supervision, Resources, Funding acquisition. **Bassam B. Dally:** Writing – review & editing, Supervision, Resources, Funding acquisition.

Declaration of competing interest

The authors declare that they have no known competing financial interests or personal relationships that could have appeared to influence the work reported in this paper.

Data availability

Data will be made available on request.

Acknowledgements

The research reported in this publication was supported by funding from The University of Adelaide, Australia, the Australian Research Council (ARC), and the Future Fuels Cooperative Research Centre (CRC), Australia.

References

[1] Evans MJ, Proud DB, Medwell PR, Pitsch H, Dally BB. Highly radiating hydrogen flames: effect of toluene concentration and phase. Proc Combust Inst 2021;38(1):1099–106.
[2] Agarwal AK. Biofuels (alcohols and biodiesel) applications as fuels for internal combustion engines. Prog Energy Combust Sci 2007;33(3):233–71.
[3] Bäckström D, Johansson R, Andersson K, Wiinikka H, Fredriksson C. On the use of alternative fuels in rotary kiln burners—An experimental and modelling study of the effect on the radiative heat transfer conditions. Fuel Process Technol 2015;138:210–20.
[4] Hutny W, Lee G. Improved radiative heat transfer from hydrogen flames. Int J Hydrog Energy 1991;16(1):47–53.
[5] Wu L, Kobayashi N, Li Z, Huang H. Numerical study of the effects of oxygen concentration and fuel jet velocity on thermal radiation in methane and propane turbulent diffusion flames. Can J Chem Eng 2015;93(9):1567–76.
[6] Reddy VM, Biswas P, Garg P, Kumar S. Combustion characteristics of biodiesel fuel in high recirculation conditions. Fuel Process. Technol. 2014;118:310–7.
[7] McEnally CS, Pfefferle LD. Sooting tendencies of oxygenated hydrocarbons in laboratory-scale flames. Environ Sci Technol 2011;45(6):2498–503.
[8] Gee AJ, Yin Y, Foo KK, Chinnici A, Smith N, Medwell PR. Toluene addition to turbulent H_2/natural gas flames in bluff-body burners. Int J Hydrog Energy 2022;47(65):27733–46.
[9] Yin Y, Medwell PR, Gee AJ, Foo KK, Dally BB. Fundamental insights into the effect of blending hydrogen flames with sooting biofuels. Fuel 2023;331:125618.
[10] Yin Y, Medwell PR, Dally BB. Hydrogen turbulent nonpremixed flames blended with spray or prevapourised biofuels. Int J Hydrog Energy 2023;48(65):25563–80.
[11] Pandey P, Pundir B, Panigrahi P. Hydrogen addition to acetylene–air laminar diffusion flames: studies on soot formation under different flow arrangements. Combust Flame 2007;148(4):249–62.
[12] Ren F, Chu H, Xiang L, Han W, Gu M. Effect of hydrogen addition on the laminar premixed combustion characteristics the main components of natural gas. J Energy Inst 2019;92(4):1178–90.
[13] Liu F, Ai Y, Kong W. Effect of hydrogen and helium addition to fuel on soot formation in an axisymmetric coflow laminar methane/air diffusion flame. Int J Hydrog Energy 2014;39(8):3936–46.
[14] Li J, Huang H, Kobayashi N, He Z, Nagai Y. Study on using hydrogen and ammonia as fuels: combustion characteristics and NO_x formation. Int J Energy Res 2014;38(9):1214–23.
[15] Park SH, Lee KM, Hwang CH. Effects of hydrogen addition on soot formation and oxidation in laminar premixed C_2H_2/air flames. Int J Hydrog Energy 2011;36(15):9304–11.
[16] Gu D, Sun Z, Dally BB, Medwell PR, Alwahabi ZT, Nathan GJ. Simultaneous measurements of gas temperature, soot volume fraction and primary particle diameter in a sooting lifted turbulent ethylene/air non-premixed flame. Combust Flame 2017;179:33–50.
[17] Celnik MS, Sander M, Raj A, West RH, Kraft M. Modelling soot formation in a premixed flame using an aromatic-site soot model and an improved oxidation rate. Proc Combust Inst 2009;32(1):639–46.
[18] Glassman I. Soot formation in combustion processes. In: Symp. (int.) combust., vol. 22, no. 1. Elsevier; 1989, p. 295–311.
[19] Li L, Sunderland PB. An improved method of smoke point normalization. Combust Sci Technol 2012;184(6):829–41.
[20] Mueller ME, Chan QN, Qamar NH, Dally BB, Pitsch H, Alwahabi ZT, et al. Experimental and computational study of soot evolution in a turbulent nonpremixed bluff body ethylene flame. Combust Flame 2013;160(7):1298–309.
[21] Wagnon SW, Thion S, Nilsson EJ, Mehl M, Serinyel Z, Zhang K, et al. Experimental and modeling studies of a biofuel surrogate compound: laminar burning velocities and jet-stirred reactor measurements of anisole. Combust Flame 2018;189:325–36.
[22] Proud DB, Evans MJ, Medwell PR, Chan QN. Experimental investigation of the flame structure of dilute sprays issuing into a hot and low-oxygen coflow. Combust Flame 2021;230:111439.
[23] Dumouchel C. On the experimental investigation on primary atomization of liquid streams. Exp Fluids 2008;45:371–422.
[24] Jenny P, Roekaerts D, Beishuizen N. Modeling of turbulent dilute spray combustion. Prog Energy Combust Sci 2012;38(6):846–87.
[25] Kourmatzis A, Pham PX, Masri AR. Characterization of atomization and combustion in moderately dense turbulent spray flames. Combust Flame 2015;162(4):978–96.
[26] Lowe A, Kourmatzis A, Masri AR. Turbulent spray flames of intermediate density: Stability and near-field structure. Combust Flame 2017;176:511–20.
[27] Zheng JL, Kong Y-P. Spray combustion properties of fast pyrolysis bio-oil produced from rice husk. Energy Convers Manag 2010;51(1):182–8.
[28] Narayanaswamy K, Pitsch H, Pepiot P. A component library framework for deriving kinetic mechanisms for multi-component fuel surrogates: application for jet fuel surrogates. Combust Flame 2016;165:288–309.
[29] Szymkowicz PG, Benajes J. Development of a diesel surrogate fuel library. Fuel 2018;222:21–34.
[30] Nowakowska M, Herbinet O, Dufour A, Glaude P-A. Kinetic study of the pyrolysis and oxidation of guaiacol. J Phys Chem A 2018;122(39):7894–909.
[31] Rahman SA, Van TC, Hossain F, Jafari M, Dowell A, Islam M, et al. Fuel properties and emission characteristics of essential oil blends in a compression ignition engine. Fuel 2019;238:440–53.
[32] Rahman S, Nabi M, Van TC, Suara K, Jafari M, Dowell A, et al. Performance and combustion characteristics analysis of multi-cylinder CI engine using essential oil blends. Energies 2018;11(4):738.
[33] Kourmatzis A, Pham PX, Masri AR. Air assisted atomization and spray density characterization of ethanol and a range of biodiesels. Fuel 2013;108:758–70.
[34] Glaude PA, Pitz WJ, Thomson MJ. Chemical kinetic modeling of dimethyl carbonate in an opposed-flow diffusion flame. Proc Combust Inst 2005;30(1):1111–8.
[35] Dayma G, Sarathy S, Togbé C, Yeung C, Thomson M, Dagaut P. Experimental and kinetic modeling of methyl octanoate oxidation in an opposed-flow diffusion flame and a jet-stirred reactor. Proc Combust Inst 2011;33(1):1037–43.
[36] Pejpichestakul W, Cuoci A, Frassoldati A, Pelucchi M, Parente A, Faravelli T. Buoyancy effect in sooting laminar premixed ethylene flame. Combust Flame 2019;205:135–46.
[37] Faravelli T, Frassoldati A, Ranzi E. Kinetic modeling of the interactions between NO and hydrocarbons in the oxidation of hydrocarbons at low temperatures. Combust Flame 2003;132(1–2):188–207.
[38] Bisetti F, Blanquart G, Mueller ME, Pitsch H. On the formation and early evolution of soot in turbulent nonpremixed flames. Combust Flame 2012;159(1):317–35.
[39] Violi A, D'Anna A, D'Alessio A. Modeling of particulate formation in combustion and pyrolysis. Chem Eng Sci 1999;54(15–16):3433–42.
[40] Buch R, Hamins A, Konishi K, Mattingly D, Kashiwagi T. Radiative emission fraction of pool fires burning silicone fluids. Combust Flame 1997;108(1–2):118–26.
[41] Wu YD, Lai DK. A density functional study of substituent effects on the O-H and O- CH3 bond dissociation energies in phenol and anisole. J Org Chem 1996;61(22):7904–10.
[42] Graziano B, Burkardt P, Neumann M, Pitsch H, Pischinger S. Development of a modified Joback–Reid Group contribution method to predict the sooting tendency of oxygenated fuels. Energy Fuels 2021;35(16):13144–58.
[43] Agrawal K, Verma AM, Kishore N. Thermochemical conversion of guaiacol in aqueous phase by density functional theory. ChemistrySelect 2019;4(20):6013–25.
[44] Bierkandt T, Hoener M, Gaiser N, Hansen N, Köhler M, Kasper T. Experimental flat flame study of monoterpenes: Insights into the combustion kinetics of α-pinene, β-pinene, and myrcene. Proc Combust Inst 2021;38(2):2431–40.
[45] Nowakowska M, Herbinet O, Dufour A, Glaude P-A. Detailed kinetic study of anisole pyrolysis and oxidation to understand tar formation during biomass combustion and gasification. Combust Flame 2014;161(6):1474–88.

[46] Andersson K, Johansson R, Johnsson F. Thermal radiation in oxy-fuel flames. Int J Greenh Gas Control 2011;5:S58–65.
[47] Ghaemi S, Rahimi P, Nobes DS. Assessment of parameters for distinguishing droplet shape in a spray field using image-based techniques. At Sprays 2009;19(9):809–31.
[48] Horiashchenko S, Horiashchenko K, Musial J. Methodology of measuring spraying the droplet flow of polymers from nozzle. Mechanics 2020;26(1):82–6.
[49] Singh G, Kourmatzis A, Masri A. Volume measurement of atomizing fragments using image slicing. Exp Therm Fluid Sci 2020;115:110102.
[50] Singh G, Kourmatzis A, Masri A. Dense sprays with a focus on atomization and turbulent combustion. Flow Turbul Combust 2021;106:405–17.
[51] Kourmatzis A, Pham PX, Masri AR. A two-angle far-field microscope imaging technique for spray flows. Meas Sci Technol 2017;28(3):035302.
[52] Comelli F, Ottani S, Francesconi R, Castellari C. Densities, viscosities, and refractive indices of binary mixtures containing n-hexane+ components of pine resins and essential oils at 298.15 K. J Chem Eng Data 2002;47(1):93–7.
[53] Ayala JR, Montero G, Campbell HE, García C, Coronado MA, León JA, et al. Extraction and characterization of orange peel essential oil from Mexico and United States of America. J Essent Oil-Bear Plants 2017;20(4):897–914.
[54] Olcese RN, François J, Bettahar M, Petitjean D, Dufour A. Hydrodeoxygenation of guaiacol, a surrogate of lignin pyrolysis vapors, over iron based catalysts: Kinetics and modeling of the lignin to aromatics integrated process. Energy Fuels 2013;27(2):975–84.
[55] Tian M, McCormick RL, Ratcliff MA, Luecke J, Yanowitz J, Glaude P-A, et al. Performance of lignin derived compounds as octane boosters. Fuel 2017;189:284–92.
[56] Jasper JJ. The surface tension of pure liquid compounds. J Phys Chem Ref Data 1972;1(4):841–1010.
[57] Vazquez G, Alvarez E, Navaza JM. Surface tension of alcohol water+ water from 20 to 50. degree. C. J Chem Eng 1995;40(3):611–4.
[58] Onyekere PF, Nnamani DO, Peculiar-Onyekere CO, Uzor PF. Limonene. In: Green sustainable process for chemical and environmental engineering and science. Elsevier; 2021, p. 219–27.